# Control of Terahertz Emission by Ultrafast Spin-Charge Current Conversion at Rashba Interfaces

Matthias B. Jungfleisch, Qi Zhang, Wei Zhang, John E. Pearson, Richard D. Schaller, Haidan Wen, and Axel Hoffmann

Phys. Rev. Lett. **120**, 207207 — Published 18 May 2018

DOI: 10.1103/PhysRevLett.120.207207

# Control of terahertz emission by ultrafast spin-charge current conversion at Rashba interfaces

Matthias B. Jungfleisch,[1,2,*] Qi Zhang,[3] Wei Zhang,[1,4] John E. Pearson,[1]
Richard D. Schaller,[5,6] Haidan Wen,[3] and Axel Hoffmann[1]

[1] *Materials Science Division, Argonne National Laboratory, Argonne, Illinois 60439, USA*
[2] *Department of Physics and Astronomy, University of Delaware, Newark, Delaware 19716, USA*
[3] *Advanced Photon Source, Argonne National Laboratory, Argonne, Illinois 60439, USA*
[4] *Department of Physics, Oakland University, Rochester, Michigan 48309, USA*
[5] *Center for Nanoscale Materials, Argonne National Laboratory, Argonne, Illinois 60439, USA*
[6] *Department of Chemistry, Northwestern University, Evanston, Illinois 60208, USA*

(Dated: March 23, 2018)

We show that a femtosecond spin current pulse can generate terahertz (THz) transients at Rashba interfaces between two non-magnetic materials. Our results unambiguously demonstrate the importance of the interface in this conversion process that we interpret in terms of the inverse Rashba Edelstein effect, in contrast to the THz emission in the bulk conversion process via inverse spin-Hall effect. Furthermore, we show that at Rashba interfaces the THz-field amplitude can be controlled by the helicity of the light. Optical generation of electric photocurrents by these interfacial effects in the femtosecond regime will open up new opportunities in ultrafast spintronics.

Terahertz (THz) spintronics has emerged as a prominent field at the boundary between magnetism, spintronics and photonics research with vast technological relevance: Ultrafast control of magnetization and spin physics as well as the development of low-cost efficient, broadband THz generators give rise to real-world applications [1]. The field of terahertz spintronics will also propel magnetic recording technologies by enabling ultrafast all-optical magnetization reversal [2–4]. Due to the transverse nature of spin transport phenomena, the spin-current generation process is generally more efficient as the cross-section of the charge current carrying layer is reduced. This motivates the search for interfacial systems as spin-charge inter-converters and to harness interfacial Rashba systems as spintronics-based THz sources.

The Rashba Edelstein effect (or inverse spin galvanic effect) [5–8] that occurs at interfaces and surfaces, can be used to interconvert spin- and charge currents [9–16]. This process can be understood as an asymmetric spin-flip scattering of electrons in systems with lifted spin degeneracy of the energy bands reflecting a broken inversion symmetry [17]. The interaction between the Pauli matrices vector $\sigma_{\rm P}$ and linear momentum $k$ can be expressed by:

$$H_{\rm R} = \alpha_{\rm R}(\vec{k} \times \vec{n})\sigma_{\rm P}, \qquad (1)$$

where $\alpha_{\rm R}$ is the Rashba coefficient and $\vec{n}$ is the unit vector normal to the interface. A charge current in a Rashba interface is associated with a nonzero spin density, which can lead to a torque acting on the magnetization in an adjacent ferromagnetic material [10, 18]. Recent spin-transport and magneto-optical Kerr effect measurements demonstrate that strong field-like torques can arise at metallic ferromagnet/normal metal bilayer interfaces [19], which stem from interfacial Rashba spin-orbit interaction. Conversely, the reverse process, known as inverse Rashba Edelstein effect, can be used to transform a nonzero spin density induced by spin injection into a charge current carried by interfacial states. This process is illustrated in Fig. 1(c): the energy bands in interfacial Rashba systems are spin-split. Spin-current injection [perpendicular to the plane in Fig. 1(c)] into those systems leads to different total occupation numbers of the two subbands. Subsequently, the Fermi contours are shifted (indicated by green arrows, $\Delta k$) leading to a non-equilibrium steady-state characterized by the generation of a charge current carried by the interfacial states. This

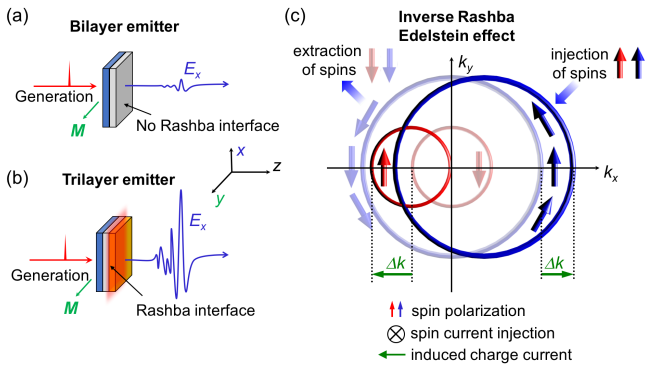


FIG. 1. (Color online) Experimental schematics and sketch of THz emission in bilayer samples, (a), and trilayer samples, where the spin-to-charge current conversion occurs at the Rashba interface between Ag and Bi, (b). The MgO substrate is facing perpendicularly to the incident femtosecond laser pulse and the magnetization $M$ is lying perpendicularly to the $x$-component of the THz-electric field, $E_{\rm x}$. The amplitude of $E_{\rm x}$ generated from the bilayer emitter, (a), is smaller than for the trilayer emitter, (b). (c) Illustration of the inverse Rashba Edelstein effect: Generation of a charge current carried by the interfacial states is due to a nonzero spin density induced by a ultrafast, pulsed spin current injection.

was recently demonstrated in transport and microwave measurements (up to a few GHz) [9–13, 20–22], but has not yet been explored in the THz regime. The proposed interface process is in contrast to the bulk effect known as inverse spin Hall effect (ISHE) [23–25] that converts laser-pulse driven spin currents into picosecond charge current bunches [26–28], which results in subsequent emission of THz electromagnetic waves.

In this Letter, we show ultrafast spin-to-charge current conversion and the generation of THz emission at interfaces between two non-magnetic materials due the inverse Rashba Edelstein effect (IREE). We demonstrate that a femtosecond spin current pulse launched from a thin CoFeB ($Co_{20}Fe_{60}B_{20}$) layer can lead to terahertz transients at a Rashba interface between two non-magnetic materials, i.e., Ag/Bi. By comparing bilayer control samples CoFeB/Ag and CoFeB/Bi with CoFeB/Ag/Bi trilayers, the importance of the interface between Ag and Bi in the terahertz generation process is revealed. We interpret our results in terms of an ultrafast spin-to-charge current conversion process at the Ag/Bi interface by means of the IREE. Ag-thickness dependent and in-plane angular-dependent measurements confirm this interpretation. We furthermore demonstrate a helicity-dependent terahertz electric field amplitude polarized parallel to the magnetization direction in the CoFeB layer.

We fabricate the samples using dc magnetron sputtering in Ar atmosphere at 5 mTorr and 30 sscm gas flow (base pressure $< 1 \times 10^{-7}$ Torr) on double-side polished MgO substrates with a (100)-orientation. The following sputtering parameters have been used: CoFeB: sputtering rate = 0.3 Å/s at 9 W, Ag: sputtering rate = 1.1 Å/s at 15 W, Bi: sputtering rate = 1.3 Å/s at 10 W, Pt: sputtering rate = 0.7 Å/s at 10 W, Al: sputtering rate = 0.75 Å/s at 75 W (Ar pressure: 3 mTorr). Seven different types of polycrystalline multilayers were grown: CoFeB(2)/Pt(2), CoFeB(2)/Ag(2)/Al(5), CoFeB(2)/Al(5), CoFeB(2)/Bi(2) and CoFeB(2)/Ag(2)/Bi(2), CoFeB(2)/Ag(4)/Bi(2), CoFeB(2)/Ag(10)/Bi(2); thickness in parenthesis in nm. We also tested a Ag(2)/Bi(2) double-layer grown on MgO without the ferromagnetic CoFeB layer. The Al layer serves as capping layer to prevent oxidation [29]. The measurement configuration is shown in Fig. 1(a,b). The incident laser pulse is aligned perpendicular to the sample plane and faces the MgO substrate ($z$-direction). A bias magnetic field of constant magnitude is applied in the sample plane ($y$-direction) to align the CoFeB magnetization $M$. The incident laser pulse is derived from a 2 kHz Ti:sapphire regenerative amplifier with 800 nm in wavelength and a pump fluence of 400 $\mu$J/cm$^2$. The generated THz field after a pair of wire-grid polarizer is measured by electro-optical sampling using a 300 $\mu$m thick (110) ZnTe crystal. More details on the experimental setup and sample characterization by atomic force microscopy

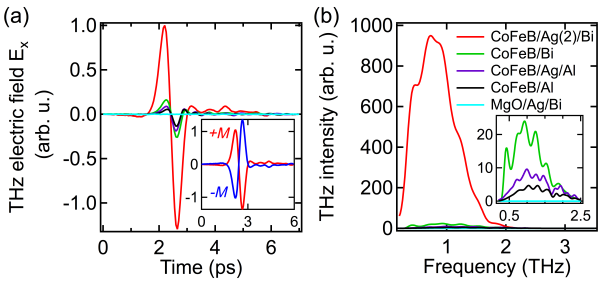


FIG. 2. (Color online) (a) Comparison of CoFeB/Ag(2)/Bi trilayer with bilayer control samples. An enhancement of the signal strength is observed when Bi is deposited on to Ag. The inset shows that the signal of CoFeB/Ag(2)/Bi is inverted when the magnetization $M$ is reversed. Please note that the signal amplitudes have been normalized to the CoFeB/Ag(2)/Bi sample. The raw data time traces can be found in the supplementary material, see Fig. S4. (b) Corresponding Fourier-transform of the time-resolved measurements shown in (a). The inset shows the THz intensity of the control samples on a magnified scale.

can be found in the supplementary material [30]. A spin current in the CoFeB layer is created by absorption of a femtosecond laser pulse that excites electrons from below the Fermi energy to bands above it. This results in a non-equilibrium electron distribution and due to the imbalance of majority-spin and minority-spin electrons, a spin-polarized electron current travels from the CoFeB into the cap layer (in $z$-direction) [26], where it is converted into a charge current bunch due to the IREE. The direction of this transient charge current is mainly perpendicular to the magnetization direction ($E_x \perp M$). The helicity dependence of the $y$-component of the THz field parallel to the magnetization ($E_y \parallel M$) is discussed in the second part of this paper.

Figure 2(a) shows terahertz signal waveforms measured from photoexcitation of the bilayer control samples and the CoFeB/Ag/Bi trilayer sample, which forms a Rashba interface between the two non-magnets Ag and Bi. As illustrated in Fig. 1(a,b) and evident from the experimental observation shown in Fig. 2(a), the $x$-component of the THz electric field of the trilayers is significantly larger than those of the bilayer control samples CoFeB/Al, CoFeB/Ag/Al, CoFeB/Bi and MgO/Ag/Bi. This observation highlights the importance of the Ag/Bi interface for the THz-generation process. No signal is found for the MgO/Ag/Bi sample where the ferromagnetic CoFeB layer is absent. A 180 degree phase shift is observed when the field polarity is reversed, see inset of Fig. 2(a). This $M$ dependence of the THz polarization supports the IREE mechanism. The Fourier spectra of the terahertz signals are shown in Fig. 2(b). The inset shows a comparison among the control samples. The CoFeB/Ag(2)/Bi covers a bandwidth (10 dB) of up to 1.65 THz, which is limited by the used ZnTe crystal (Control measurements

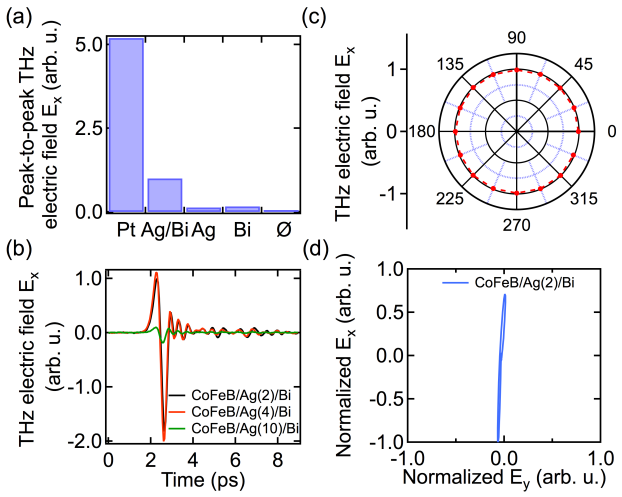


FIG. 3. (Color online) (a) Comparison of THz amplitude for different sample stacks. The signal strength of the benchmark spin-to-charge converter Pt exceeds the one of the IREE-based trilayer system. An enhancement of the signal strength with respect to the control samples (CoFeB/Ag/Al denoted as Ag, CoFeB/Bi denoted as Bi and CoFeB/Al denoted as ø) is observed for the Ag/Bi system. (b) Comparison of the temporal evolution of the THz electric field $E_x$ in $x$-direction for three different Ag thicknesses. (c) The peak THz electric field as a function of the the rotation of the laser polarization. Please note that the signal amplitudes have been normalized to the CoFeB/Ag(2)/Bi sample in (a-c). The raw data time traces can be found in the supplementary material, Fig. S4. (d) Parametric plot of THz electric field amplitude. The generated THz signal is mainly polarized along the $x$-direction.

using a GaP detector crystal confirmed a bandwidth of up to approximately 2.2 THz). From Fig. 2(b) it is apparent that the THz-intensity of the CoFeB/Ag(2)/Bi sample exceeds the value of the control samples by a factor of approximately two orders of magnitude. A comparison between our IREE-based THz emitter (Ag/Bi Rashba interface) and the benchmark ISHE-emitter Pt is shown in the supplementary material, Fig. S2. The signal waveform and the spectra of the various samples, including the ISHE-based emitter Pt, are very similar. From our measurements, we can conclude that the IREE process can be as fast as sub-ps, which sets the lower bound speed for the conversion process [31].

Figure 3(a) shows a comparison of the THz electric field in $x$-direction generated from the various samples. It highlights the importance of the non-magnetic layers deposited on the CoFeB layer for the THz-generation process: When Ag and Bi are deposited on top of the CoFeB layer, an enhancement by a factor of approximately 6 is observed in comparison to the bilayer control samples. Please note that the Al capping layer, which has a trivial spin Hall effect, prevents the layer underneath it from oxidation and is not expected to alter the generation of THz-radiation. The result of CoFeB/Pt is shown for comparison. Our CoFeB/Ag(2)/Bi trilayer system is a factor of 5 smaller than the Pt reference sample, where the spin-to-charge conversion is due to the ISHE.

The Rashba-coupling at the interface between Ag and Bi leads to a spin splitting of the energy bands, which is necessary for the spin-charge interconversion, Fig. 1(c). The control samples, which do not include this interface are therefore not expected to show any THz emission. However, we do observe a smaller, yet noticeable, signal from the CoFeB-based control samples (see Fig. 2). We emphasize that the MgO/Ag/Bi sample does not show any signal, which means that THz emission in the control samples is related to magnetism in CoFeB. Although the weak THz emission from these control samples is not the focus of this work, we propose three possible contributions, which indicate a different generation mechanism of the $E_x$ component: (1) The IREE can occur at surfaces when space inversion symmetry is broken. This requirement is also fulfilled for the control samples. (2) CoFeB itself may show a non-zero spin-Hall angle resulting in spin-charge conversion in the CoFeB layer [32–34]. (3) Ultrafast demagnetization in the CoFeB layer can lead to THz radiation [1].

Our results show an ultrafast spin-to-charge current conversion at the Ag/Bi interface due to the IREE, which was previously studied in electrical transport *and* dynamic (GHz frequency range) measurements [9–14, 18] and demonstrate that this conversion process persists on much faster time scales. In order to further validate the IREE mechanism, we measured the thickness-dependence of the Ag-interlayer in the trilayer system. Figure 3(b) shows a comparison of the temporal evolution of the THz electric field $E_x$ for three different Ag thicknesses. As is apparent, the samples with 2 nm and 4 nm thick Ag sandwiched between CoFeB and Bi show almost the same signal strength. The 10 nm thick Ag interlayer, however, exhibits a drastically reduced signal strength. While the general trend qualitatively agrees with what we would expect for spin diffusion through Ag, it does not match quantitatively. Further studies are required to understand the details of the thickness dependence. Our observation nonetheless underlines the importance of the interface between Ag and Bi for the THz generation process. Figure 3(c) shows the peak THz electric field as a function of the rotation of the laser polarization and will be discussed in detail below.

Figure 3(d) shows a parametric plot of the THz field amplitude. As is apparent from the figure, the THz emission is mainly polarized in $x$-direction perpendicular to the magnetization. However, we observe a small component with a magnitude of a few percent of $E_x$ parallel to the magnetization in $y$-direction, $E_y$. Figure 4(a) illustrates the two orthogonal components $E_x$ and $E_y$.

In the following, we will show that the $y$-component of the THz field created in the trilayer CoFeB/Ag(2)/Bi

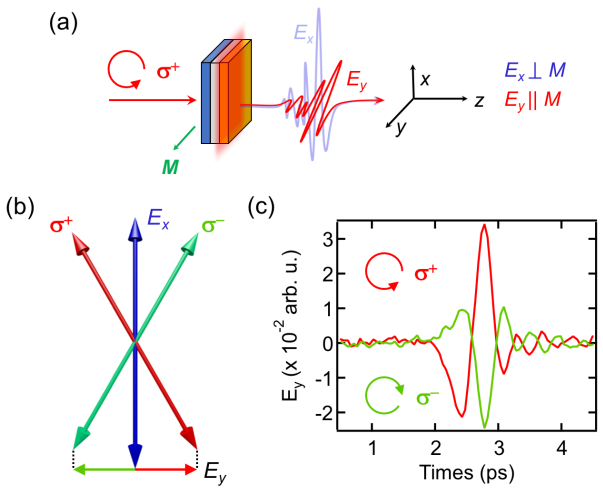


FIG. 4. (Color online) (a) Illustration of $x$- and $y$-component of the THz electric field (b) Sketch of helicity-dependent $y$-component of the THz amplitude. $E_{\mathrm{y}}$ is oriented parallel to the magnetization $M$. (c) Time traces of $y$-component of THz electric field $E_{\mathrm{y}}$ for right-circularity/left-circularly polarized laser light respectively. Result was obtained from CoFeB/Ag(2)/Bi. Please note that the signal amplitude has been normalized to the maximum of the THz electric field in $x$-direction.

[see Fig. 4(a)] can be controlled by the helicity of the laser pump. Interfacial Rashba-coupling allows for a coherent transfer of angular momentum in the ultrafast spin-charge conversion process due to the IREE. This helicity-dependent control is only observable for interfacial Rashba samples, and although the $x$-component of the THz signal $E_{\mathrm{x}}$ of CoFeB/Pt is much stronger, we do not find any helicity-dependence in its $y$-component. Dependent on the helicity of the light the polarization direction changes as shown in Fig. 4(b), which experimentally results in an increase in the $y$-component of the electric field amplitude $E_{\mathrm{y}}$ for left-circularly ($\sigma^+$) polarized light and in a decrease for a right-circularly polarized light ($\sigma^-$). The time traces of $E_{\mathrm{y}}$ for $\sigma^-$ and $\sigma^+$ polarized light are shown in Fig. 4(c), CoFeB/Ag(2)/Bi. As is apparent, the electric field of the emitted terahertz radiation can be controlled by the helicity: A 180 degree phase shift is obtained between $\sigma^+$ and $\sigma^-$ light. We emphasize that the control samples CoFeB/Al, CoFeB/Bi and CoFeB/Ag/Al and CoFeB/Pt (which shows the largest signal in $E_{\mathrm{x}}$) did not show any helicity-dependence in $y$-direction. Furthermore, it is important to note that no helicity-dependent THz emission in the $x$-component was found for CoFeB/Ag(2)/Bi or any of the control samples. The thinner Ag interlayers of 2 nm and 4 nm showed clear and consistent helicity dependence. The signal strength in the $y$-component of the CoFeB/Ag(10)/Bi was too small to determine whether there is a dependence on helicity or not. We can exclude a helicity-dependent absorption of light since the magnitude of the $E_{\mathrm{x}}$ component is not affected by the helicity of the optical pump pulse.

A spin-charge current conversion based on IREE (as well as ISHE) is expected to only create a THz polarization perpendicular to the magnetization ($x$-direction). Clearly, we also observe a polarization parallel to the magnetization ($y$-direction). However, the signal strength in $y$-direction is drastically reduced compared to the $x$-direction. The ratio between both components is $E_{\mathrm{y}}/E_{\mathrm{x}} \approx 0.03$. A possible scenario for our observation is a contribution from the inverse Faraday effect. The inverse Faraday effect is expected to show a helicity-dependent component of the THz signal parallel to the magnetization $\vec{j} \propto \vec{m} \times (\vec{M} \times \vec{\sigma})$ [35], where $\vec{j}$ is the photocurrent, $\vec{n}$ is the unit vector normal to the interface, $\vec{M}$ is the magnetization and $\vec{\sigma}$ is the axial unit vector parallel or antiparallel to the propagation of light. This effect might also contribute to THz emission along the $y$-axis. However, contrary to the observation in Ref. [35] for Co/Pt, we do not see any helicity-dependent THz emission in $y$-direction (parallel to the magnetization) for any of the control samples including CoFeB/Pt. Furthermore, the largest ratio between $x$- and $y$-polarization we find in CoFeB/Ag/Bi is $E_{\mathrm{y}}/E_{\mathrm{x}} \approx 0.03$, which is 5 times smaller than the biggest value reported in Ref. [35].

These observations demonstrate the control of THz emission by the helicity of the pump light, which is in contrast to the pump-polarization independence during IREE process shown in Fig. 3(c). This highlights the complexity of spin-current conversion at Rashba interfaces and motivates future studies of coherent light control of spin transport processes at interfaces. Figure 3(c) shows the peak THz electric field polarized in $x$-direction as a function of the pump laser polarization rotation with respect to the $x$-axis (Ag thickness = 2 nm). We observe an almost constant THz electric field $E_{\mathrm{x}}$ when the polarization is rotated. This observation shows that the THz signal as generated by IREE does not depend on the electric field of the laser pump pulse. We also tested the THz emission for different in-plane sample orientations while laser polarization was fixed and the magnetic field direction was kept constant (not shown). No dependence was found, which implies that the THz signal from the magnetic heterostructure is independent on the magnetic or crystalline anisotropy. Please note that the laser power for the rotational measurements was reduced resulting in a smaller magnitude of the THz electric field.

In summary, we have shown that a femtosecond spin current pulse can generate terahertz transients at Rashba interfaces between two non-magnetic materials, i.e., Ag/Bi. Our results demonstrate an enhancement of THz-emission by a factor of 6 when a bilayer of Ag/Bi is deposited onto the metallic ferromagnet CoFeB highlighting the importance of the interface between Ag and Bi. We understand our results as a conversion of the photoexcited spin-current pulse into a charge-current bunch

by the inverse Rashba Edelstein effect. Furthermore, we demonstrated a helicity-dependent THz-electric field that is polarized parallel to the CoFeB magnetization direction. This effect is absent in the control samples (CoFeB/Ag, CoFeB/Bi, CoFeB, CoFeB/Pt) and is most pronounced for thinner Ag layers below 10 nm. We anticipate that optical generation of electric photocurrents by these kind of interfacial effects in the femtosecond regime will open up new possibilities in ultrafast spintronics and stimulate further experimental and theoretical research endeavors. The observed ultrafast generation and control of currents at the interfaces of non-magnetic materials might lead to spintronics applications and devices where picosecond current pulses can be manipulated wirelessly by the helicity of light.

We thank T. Kampfrath, K. Roy, R. Winkler and W. Jiang for valuable discussions. This work was supported by the U.S. Department of Energy, Office of Science, Materials Science and Engineering Division. The use of Center for Nanoscale Materials is supported by DOE-BES, under Contract No. DE-AC02-06CH11357.

* jungfleisch@anl.gov

[1] J. Walowski and M. Münzenberg, J. Appl. Phys **120**, 140901 (2016).
[2] C.-H. Lambert, S. Mangin, B. S. D. C. S. Varaprasad, Y. K. Takahashi, M. Hehn, M. Cinchetti, G. Malinowski, K. Hono, Y. Fainman, M. Aeschlimann, and E. E. Fullerton, Science **345**, 1337 (2014).
[3] S. Mangin, M. Gottwald, C.-H. Lambert, D. Steil, V. Uhlíř, L. Pang, M. Hehn, S. Alebrand, M. Cinchetti, G. Malinowski, Y. Fainman, M. Aeschlimann, and E. E. Fullerton, Nature Materials **13**, 286 (2014).
[4] C. D. Stanciu, F. Hansteen, A. V. Kimel, A. Kirilyuk, A. Tsukamoto, A. Itoh, and T. Rasing, Phys. Rev. Lett. **99**, 047601 (2007).
[5] D. Culcer and R. Winkler, Phys. Rev. Lett. **99**, 226601 (2007).
[6] E. L. Ivchenko and G. Pikus, JETP Lett. (1978).
[7] V. M. Edelstein, Solid State Communications **73**, 233 (1990).
[8] A. Manchon, H. C. Koo, J. Nitta, S. M. Frolov, and R. A. Duine, Nature Materials **14**, 871 (2015).
[9] J. C. R. Sánchez, L. Vila, G. Desfonds, S. Gambarelli, J. P. Attane, J. M. De Teresa, C. Magén, and A. Fert, Nature Communications **4**, 459 (2013).
[10] M. B. Jungfleisch, W. Zhang, J. Sklenar, W. Jiang, J. E. Pearson, J. B. Ketterson, and A. Hoffmann, Phys. Rev. B **93**, 224419 (2016).
[11] W. Zhang, M. B. Jungfleisch, W. Jiang, J. E. Pearson, and A. Hoffmann, J. Appl. Phys **117**, 17C727 (2015).
[12] S. Sangiao, J. M. De Teresa, L. Morellon, I. Lucas, M. C. Martinez-Velarte, and M. Viret, Appl. Phys. Lett. **106**, 172403 (2015).
[13] M. Isasa, M. C. Martinez-Velarte, E. Villamor, C. Magén, L. Morellón, J. M. De Teresa, M. R. Ibarra, G. Vignale, E. V. Chulkov, E. E. Krasovskii, L. E. Hueso, and F. Casanova, Phys. Rev. B **93**, 014420 (2016).
[14] J. Sklenar, W. Zhang, M. B. Jungfleisch, W. Jiang, H. Saglam, J. E. Pearson, J. B. Ketterson, and A. Hoffmann, J. Appl. Phys **120**, 180901 (2016).
[15] A. Soumyanarayanan, N. Reyren, A. Fert, and C. Panagopoulos, Nature **539**, 509 (2016).
[16] F. Hellman, A. Hoffmann, Y. Tserkovnyak, G. S. D. Beach, E. E. Fullerton, C. Leighton, A. H. MacDonald, D. C. Ralph, D. A. Arena, H. A. Dürr, P. Fischer, J. Grollier, J. P. Heremans, T. Jungwirth, A. V. Kimel, B. Koopmans, I. N. Krivorotov, S. J. May, A. K. Petford-Long, J. M. Rondinelli, N. Samarth, I. K. Schuller, A. N. Slavin, M. D. Stiles, O. Tchernyshyov, A. Thiaville, and B. L. Zink, Rev. Mod. Phys. **89**, 1293 (2017).
[17] M. B. Jungfleisch, W. Zhang, R. Winkler, and A. Hoffmann, Spin-Orbit Torques and Spin Dynamics, In: Dyakonov M. (eds) Spin Physics in Semiconductors, Springer Series in Solid-State Sciences, vol 157 (Springer, Cham, 2017).
[18] H. Nakayama, Y. Kanno, H. An, T. Tashiro, S. Haku, A. Nomura, and K. Ando, Phys. Rev. Lett. **117**, 116602 (2016).
[19] X. Fan, H. Celik, J. Wu, C. Ni, K.-J. Lee, V. O. Lorenz, and J. Q. Xiao, Nature Communications **5**, 579 (2014).
[20] Q. Song, H. Zhang, T. Su, W. Yuan, Y. Chen, W. Xing, J. Shi, J. Sun, and W. Han, Science Advances **3**, e1602312 (2017).
[21] E. Lesne, Y. Fu, S. Oyarzun, J. C. Rojas-Sanchez, D. C. Vaz, H. Naganuma, G. Sicoli, J. P. Attane, M. Jamet, E. Jacquet, J. M. George, A. Barthélémy, H. Jaffres, A. Fert, M. Bibes, and L. Vila, Nature Materials **15**, 1261 (2016).
[22] M. Matsushima, Y. Ando, S. Dushenko, R. Ohshima, R. Kumamoto, T. Shinjo, and M. Shiraishi, Appl. Phys. Lett. **110**, 072404 (2017).
[23] J. E. Hirsch, Phys. Rev. Lett. **83**, 1834 (1999).
[24] A. Hoffmann, IEEE Transactions on Magnetics **49**, 5172 (2013).
[25] M. B. Jungfleisch, W. Zhang, W. Jiang, and A. Hoffmann, SPIN **05**, 1530005 (2015).
[26] T. Kampfrath, M. Battiato, P. Maldonado, G. Eilers, J. Nötzold, S. Mährlein, V. Zbarsky, F. Freimuth, Y. Mokrousov, S. Blügel, M. Wolf, I. Radu, P. M. Oppeneer, and M. Münzenberg, Nat. Nanotechnol. **8**, 256 (2013).
[27] T. Seifert, S. Jaiswal, U. Martens, J. Hannegan, L. Braun, P. Maldonado, F. Freimuth, A. Kronenberg, J. Henrizi, I. Radu, E. Beaurepaire, Y. Mokrousov, P. M. Oppeneer, M. Jourdan, G. Jakob, D. Turchinovich, L. M. Hayden, M. Wolf, M. Münzenberg, M. Kläui, and T. Kampfrath, Nat. Photon. **10**, 483 (2016).
[28] D. Yang, J. Liang, C. Zhou, L. Sun, R. Zheng, S. Luo, Y. Wu, and J. Qi, Adv. Opt. Mater. (2016).
[29] G. Mihajlović, D. K. Schreiber, Y. Liu, J. E. Pearson, S. D. Bader, A. K. Petford-Long, and A. Hoffmann, Appl. Phys. Lett. **97**, 112502 (2010).
[30] The supplementary material contains further information on the experimental setup, a comparison of IREE-based and ISHE-based THz emitters, atomic force microscopy images, and the raw data time traces of different sample sets.
[31] S. Zhang and A. Fert, Phys. Rev. B **94**, 184423 (2016).
[32] A. Tsukahara, Y. Ando, Y. Kitamura, H. Emoto, E. Shikoh, M. P. Delmo, T. Shinjo, and M. Shiraishi,

Phys. Rev. B **89**, 235317 (2014).
[33] A. Azevedo, O. A. Santos, R. O. Cunha, R. Rodríguez-Suárez, and S. M. Rezende, Appl. Phys. Lett. **104**, 152408 (2014).
[34] M. Weiler, J. M. Shaw, H. T. Nembach, and T. J. Silva, IEEE Magn. Lett. **5**, 1 (2014).
[35] T. J. Huisman, R. V. Mikhaylovskiy, J. D. Costa, F. Freimuth, E. Paz, J. Ventura, P. P. Freitas, S. Blügel, Y. Mokrousov, T. Rasing, and A. V. Kimel, Nat. Nanotechnol. **11**, 455 (2016).